Journal of Applied Fluid Mechanics, Vol. 15, No. 4, pp. 1137-1153, 2022.
Available online at www.jafmonline.net, ISSN 1735-3572, EISSN 1735-3645.
https://doi.org/10.47176/jafm.15.04.33354

Computational Investigation of Effects of Side-Injection Geometry on Thrust-Vectoring Performance in a Fuel-Injected Dual Throat Nozzle

M. R. Salimi[1†], R. Askari[2] and M. Hasani[3]

[1] *Aerospace Research Institute, Tehran, Iran*
[2] *Aerospace Engineering, Independent Researcher*
[3] *University of Shahid Satari, Tehran, Iran*

†Corresponding Author Email:mohammadsalimi@ari.ac.ir

(Received September 8, 2021; accepted March 23, 2022)

ABSTRACT

Dual-throat Nozzle (DTN) is known as one of the most effective approaches of fluidic thrust-vectoring. It is gradually flourishing into a promising technology to implement supersonic and hypersonic thrust-vector control in aircrafts. The main objective of the present study is numerical investigation of the effects of secondary injection geometry on the performance of a fuel-injected planar dual throat thrust-vectoring nozzle. The main contributions of the study is to consider slot and circular geometries as injector cross-sections for injecting four different fuels; moreover, the impact of center-to-center distance of injection holes for circular injector is examined. Three-dimensional compressible reacting simulations have been conducted in order to resolve the flowfield in a dual throat nozzle with pressure ratio of 4.0. Favre-averaged momentum, energy and species equations are solved along with the standard $k-\varepsilon$ model for the turbulence closure, and the eddy dissipation model (EDM) for the combustion modelling. Second-order upwind numerical scheme is employed to discretize and solve governing equations. Different assessment parameters such as discharge coefficient, thrust ratio, thrust-vector angle and thrust-vectoring efficiency are invoked to analyze the nozzle performance. Computationally predicted data are agreed well with experimental measurements of previous studies. Results reveal that a maximum vector angle of 17.1 degrees is achieved via slot injection of methane fuel at a secondary injection rate equal to 9% of primary flow rate. Slot injection is performing better in terms of discharge coefficient, thrust-vector angle and thrust-vectoring efficiency, whereas circular injection provides higher thrust ratio. At 2% secondary injection for methane fuel, vector angle and vectoring efficiency obtained by slot injector is 8% and 34% higher than the circular injector, respectively. Findings suggest that light fuels offer higher thrust ratio, vector angle and vectoring efficiency, while heavy fuels have better discharge coefficient. Increasing center-to-center distance of injector holes improves thrust ratio, while having a negative effect on discharge coefficient, vector angle and vectoring efficiency. A comparison between fuel injectant of current study and inert injectant in the previous studies indicates that fuel reaction could exhibit substantial positive effects on vectoring performance. Secondary-to-primary momentum flux ratio is found to play a crucial role in nozzle performance.

Keywords: Dual throat nozzle; Fuel injection; Injection geometry; Thrust-vector angle; Thrust-vectoring efficiency.

NOMENCLATURE

A_{throat}	nozzle throat area	h	enthalpy
C_d	discharge coefficient of nozzle	h_k	enthalpy of k'th species
C_f	system resultant thrust ratio	$h^\circ_{f,k}$	standard formation enthalpy of k'th species
$C_{p,k}$	specific heat at constant pressure	J_k	diffusion flux of k'th species
C_μ	model constant	k	turbulence kinetic energy
F_a	axial thrust	M_k	molecular weight of k'th species
F_{ip}	ideal isentropic thrust of primary nozzle	NPR	nozzle pressure ratio
F_{is}	ideal isentropic thrust of secondary nozzle	P	pressure
F_n	normal thrust	$P_{ambient}$	ambient pressure
F_r	resultant thrust	P_0	stagnation pressure

$\dot{Q}$	heat release rate
R	air gas constant
R_u	universal gas constant
Sc	Schmidt number
T	temperature
T_0	stagnation temperature
u_i	velocity component in the i'th direction
w_p	weight flow rate of primary jet
w_s	weight flow rate of secondary jet
w_{ip}	ideal weight flow of primary nozzle
x_i	coordinates of the i'th direction
Y_k	mass fraction of k'th species
γ	specific heats ratio
δ_p	resultant pitch thrust-vector angle
ε	dissipation rate of turbulence kinetic energy
η	resultant pitch thrust vectoring efficiency
λ	conductivity
μ	molecular dynamic viscosity
μ_t	turbulence dynamic viscosity
ν	stoichiometric coefficient
ρ	density
σ_ε	turbulence Prandtl numbers for ε
σ_k	turbulence Prandtl numbers for k
τ	shear stress
ϕ	secondary injection percentage from total mass flow rate
$\dot{\omega}_k$	net rate of production of k'th species

1. INTRODUCTION

Fluidic thrust-vectoring has been employed for decades as a means for designing fixed-geometry nozzles with a performance comparable to variable-geometry nozzles. In fluidic methods, side-injection of a secondary fluid is performed in order to vector the mainstream jet at the nozzle outlet, while variable-geometry nozzles employ mechanical devices to change and control the direction of main jet. Due to utilizing fixed geometry and less need for complicated mechanical devices, fluidic methods have reduced the nozzle weight and manufacturing complexities.

Shock-vector control, throat skewing and counterflow method are three major fluidic techniques of thrust-vectoring, which have been traditionally used (Flamm *et al*. 2007; Anderson *et al*. 1997; Giuliano *et al*. 1997; Waithe and Deere 2003; Deere 1998; Hunter and Deere 1999; Deere 2000; Wing 1994; Wing and Giuliano 1997; Federspiel *et al*. 1995). Thrust ratio and thrust-vectoring efficiency are commonly used to evaluate fluidic methods performance. Thrust ratio is defined as the ratio of real resultant thrust to ideal thrust, while thrust-vectoring efficiency is expressed as the ratio of thrust-vector angle to secondary injection percentage of total nozzle flow. Shock-vector control in which injection occurs at the downstream of the nozzle throat, offers considerable vectoring angles, while reducing the thrust ratio (Deere 2003). A nozzle with shock-vectoring (Wing 1994) has achieved a vectoring angle of 17.3 degrees at the nozzle pressure ratio (NPR) of 4, however thrust ratio lies between 0.84 and 0.9 and vectoring efficiency takes values between 1.8 to 3.0 degrees per percent secondary injection. In another study pertaining shock-vectoring, Forghany *et al*. (2017) numerically investigated the impact of secondary injection angle varied from 60 to 120 degrees in a convergent-divergent nozzle at different aerodynamic and geometric conditions. Their findings revealed that injection angle provides substantial effects on shock-vectoring performance. Furthermore, they showed that both the reduction of nozzle expansion ratio and increment of nozzle pressure ratio leave negative effects on thrust-vector angle and thrust-vectoring efficiency. In order to achieve higher thrust ratios, throat-skewing technique is recommended due to absence of shock losses associated with shock-vectoring. A throat-skewing nozzle (Yagle *et al*. 2000) has achieved vectoring efficiencies between 2.0 (at the NPR=5.5) and 3.9 (at the NPR=2.0), while thrust ratio takes values as good as between 0.945 and 0.975. Counterflow technique in which flow suction is performed in a secondary duct near throat, provides good vectoring angles even with low secondary injection rates, but faces issues like suction supply source (Flamm 1998). Additionally, some innovations are also made to accomplish flow deflection in convergent-divergent nozzles, which seem to provide some advantages. Thillaikumar *et al*. (2020) suggested installing a strut in the divergent portion of a nozzle in order to deflect exhaust gas with no need to fluid injection. Their experiments indicated that installing a strut with a height of 3.5 mm at the x=0.72L away from the throat location, will offer the most effective thrust-vectoring with a maximum deflection angle of 3.6 degrees at NPR=4.

A new fluidic technique has been developed by Deere *et al*. (2005) at the NASA Langley Research Center. This technique is a convergent-divergent-convergent nozzle with two geometric minimum cross sections (throats), denoted as "dual throats". A cavity is created between two throats. A side-injection port is devised at the upstream throat from which a secondary flow is injected asymmetrically. Therefore, a new aerodynamic minimum area is created between the throats and the sonic plane is shifted. Mainstream is deflected towards the cavity in the opposite side of the secondary injection. Then, the final convergent section of the nozzle redirects the main jet back toward the injection side of the nozzle. Presence of cavities establishes a separated flow region within the cavity. Thus, a low-pressure recirculation flow zone is formed inside the cavity. On the other hand, the opposite side cavity is filled with the high-velocity high-pressure fluid, which dramatically increases the pressure on the wall. Low pressure in one cavity and high pressure in the other cavity enhance thrust-vectoring. The main advantage of dual-throat nozzles is the higher vectoring efficiency compared

to previous techniques. Vectoring efficiencies as high as 7.7 degrees per percent secondary injection are experimentally achieved by DTNs, whereas the highest efficiency for throat-skewing is 3.9 and for shock-vectoring is 4.5 (Deere *et al*. 2005).

Flamm *et al*. (2005) in continuation of researches launched in Langley Research Center, experimented a DTN in different operational conditions. They investigated the impacts of cavity length and secondary injection angle on nozzle performance for a two-dimensional DTN with NPR's in the range of 2.0 to 10.0. Their results revealed that the maximum vectoring angle is 15 degrees which is achieved at the NPR=4. The maximum vectoring efficiency is 6.1 degrees per percent secondary injection, which occurs at the NPR=4 and 1% secondary injection. Meanwhile, thrust ratio is 0.968, which is only 0.5% lower than a case without side injection. The same research group in another study (Flamm *et al*. 2007), experimentally investigated an axisymmetric DTN. Geometrical parameters such as cavity length, nozzle expansion ratio, circumferential span of injection and cavity convergence angle were investigated in their study. NPR and secondary injection rate were varied from zero up to 10 and 10%, respectively. Their results revealed that a 60 degree span of injection provides a better performance than 90 degree span. For secondary injection rates below 7%, the vectoring angle for 60 degree span is 1.5-2.0 times greater than 90 degree span. Reducing the cavity length improves discharge coefficient and thrust ratio, while impairs vectoring angle and efficiency. Increasing cavity convergence angle from 20 degrees to 30 degrees improves vectoring angle by 1 degree, whereas having a negative effect on discharge coefficient and thrust ratio. The best nozzle performance is achieved at a nozzle expansion ratio equal to 1. The mentioned research group have conducted other studies (Deere *et al*. 2007; Flamm *et al*. 2006; Deere *et al*. 2003) which interested reader is referred to.

In a recent study Hamedi *et al*. (2015) have investigated the effect of side-injection slot width on the nozzle performance. Their results showed that reducing the slot width enhances vectoring angle and efficiency. Wu *et al*. (2021) numerically investigated the impact of NPR, secondary to primary momentum flux ratio and secondary injection angle on the performance of DTN. Their results revealed that increasing NPR improves thrust ratio and vectoring efficiency and reduces vectoring angle. Furthermore, increasing the momentum flux ratio impairs thrust ratio and vectoring efficiency and boosts vectoring angle. A secondary injection angle of 150 degrees is found to provide the best performance in terms of thrust ratio and vectoring efficiency.

Gu and Xu (2014), Gu and Xu (2015) and Gu *et al* (2014) proposed using bypass flow instead of side-injection in DTN nozzles. The results showed that employing a bypass flow removes need to side-injection in DTN nozzles. While, in the same operational conditions, the performance of bypass DTN in terms of vectoring efficiency is similar to best performance of typical DTN's or other fluidic techniques. Furthermore, the vectoring angle of bypass DTN is higher than reported typical DTN's. Specifically, at NPR=10, the bypass DTN achieves a vectoring angle of 21.3 degrees. In continuation of bypass DTN researches, Wang *et al*. (2020a) and Wang *et al*. (2020b) investigated an axisymmetric DTN. Their results showed that a maximum thrust ratio of 0.94 and a maximum vectoring angle of 19.52 degrees are achieved at NPR=4.47, while discharge coefficient having a value of 0.97. In the most recent studies in this area, Hamedi *et al*. (2020a,b) investigated the impact of location of bypass duct on the performance of DTN. Their results showed that installing bypass duct at the upstream throat provides the best performance. Furthermore, discharge coefficient is between 0.85 and 0.93 for the NPR in the range of 2.0-4.0.

Dual-throat nozzle as a futuristic technology for thrust vectoring systems, has attracted wide interest due to its promising capabilities and great potential to be implemented in high maneuverable fighter aircrafts. It has attained thrust vectoring efficiencies higher than any other reported fluidic thrust vectoring method. The main focus of previous studies has been on optimization of the geometrical parameters of DTN. Therefore inert fluids such as air has been used as the side-injectant, and injection of reactive fluids such as hydrocarbon fuels hasn't been paid any attention in the context of DTN's. The main objective of the present study is investigation of the performance of a fuel-injected DTN. Using reactive injectants such as hydrocarbons could dramatically affect the nozzle performance due to effects of heat release and volume expansion. The effects of geometry of fuel injection ports is evaluated using different parameters such as discharge coefficient, thrust ratio, thrust-vector angle and thrust-vectoring efficiency, while the findings are compared to the previous observations from inert injectants. The study is focused on slot and circular geometries as injector cross-sections, while center-to-center distance of injector holes for circular injection is varied from 0.09" to 0.27". Four fuels consisting of two light and two heavy hydrocarbons are taken into account as injectants. The novelties of the current paper, which are not addressed in the preceding researches, are (a) using four different hydrocarbon fuels instead of air as side-injactant, (b) using slot and circular ports with variable center-to-center distance for injection.

2. GOVERNING EQUATIONS

The jet flow within the DTN of the current study is considered to be steady, three-dimensional, compressible and fully turbulent. Density is provided by ideal-gas equation. Molecular viscosity is considered as a function of temperature and obtained by the Sutherland equation. The gravity effects are neglected due to jet high velocity. Based on the mentioned assumptions, the Favre-averaged transport equations can be expressed as (Chen *et al*. 2016):

Continuity equation:

$$\frac{\partial(\rho u_i)}{\partial x_i} = 0 \tag{1}$$

Momentum equations:

$$\frac{\partial(\rho u_i u_j)}{\partial x_j} = -\frac{\partial p}{\partial x_i} + \frac{\partial}{\partial x_j}\left(\tau_{ji} - \langle \rho u_i' u_j' \rangle\right) \tag{2}$$

Chemical species transport equations:

$$\frac{\partial(\rho u_i Y_k)}{\partial x_i} = -\frac{\partial}{\partial x_i} J_k + \dot{\omega}_k \tag{3}$$

Energy equation:

$$\frac{\partial(\rho u_i h)}{\partial x_i} = u_i \frac{\partial p}{\partial x_i} + \frac{\partial}{\partial x_i}\left[(\lambda + \lambda_t)\frac{\partial T}{\partial x_i}\right] - \sum_{k=1}^{N} \frac{\partial}{\partial x_i} h_k J_k + \frac{\partial\left(u_i \tau_{ij}\right)}{\partial x_i} + \dot{Q} \tag{4}$$

Diffusion flux for k'th species:

$$J_k = -\left(\rho D_{m,k} + \frac{\mu_t}{Sc_t}\right)\frac{\partial Y_k}{\partial x_i} - \frac{D_{T,k}}{T}\frac{\partial T}{\partial x_i} \tag{5}$$

Gas mixture enthalpy:

$$h = \sum_{k=1}^{N} h_k Y_k \tag{6}$$

Where the enthalpy for k'th species is defined as:

$$h_k = h^{\circ}_{f,k} + \int_{T^0}^{T} C_{p,k} dT \tag{7}$$

The set of equations would be complete with the ideal-gas equation and overall continuity of species:

$$p = \rho R_u T \sum_{k=1}^{N} \left(\frac{Y_k}{M_k}\right) \tag{8}$$

$$\sum_{k=1}^{N} (Y_k) = 1 \tag{9}$$

RANS approach has been employed in several investigations related to the dual-throat nozzles among which references (Hamedi *et al*. 2020a and 2021b, Gu *et al*. 2014, and Deere and Karen. 2003) can be mentioned as some examples. In these researches, reliable results were obtained by steady RANS approach, which compelled us to utilize this method.

The $k-\varepsilon$ turbulence model due to its suitable accuracy and low computational cost has been a popular model for simulating reacting flows (which are inherently expensive). This model has been used in numerous reacting flow simulations in various geometries and has produced reliable results, some of which can be observed in references (Giuffrida *et al*. 2020, Berni *et al*. 2021, Verma *et al* 2021, Aleiferis *et al*. 2021, Bordoloi *et al*. 2021 and Ong *et al*. 2021). In this model, the Reynolds stresses can be related to turbulent viscosity as follows:

$$-\langle \rho u_i' u_j' \rangle = \mu_t \left(\frac{\partial u_i}{\partial x_j} + \frac{\partial u_j}{\partial x_i}\right) - \frac{2}{3}\left(\rho k + \mu_t \frac{\partial u_k}{\partial x_k}\right)\delta_{ij} \tag{10}$$

Where μ_t is the turbulent viscosity and is obtained as:

$$\mu_t = \rho C_\mu k^2/\varepsilon \tag{11}$$

Where $C_\mu = 0.09$ is one of the model constants. Transport equations for turbulence kinetic energy (k) and it's dissipation rate (ε) are expressed as:

$$\frac{\partial(\rho u_i k)}{\partial x_i} = \frac{\partial}{\partial x_i}\left[\left(\mu + \frac{\mu_t}{\sigma_k}\right)\frac{\partial k}{\partial x_i}\right] + G_k - Y_k \tag{12}$$

$$\frac{\partial(\rho u_i \varepsilon)}{\partial x_i} = \frac{\partial}{\partial x_i}\left[\left(\mu + \frac{\mu_t}{\sigma_\varepsilon}\right)\frac{\partial \varepsilon}{\partial x_i}\right] + G_\varepsilon - Y_\varepsilon \tag{13}$$

Where σ_k and σ_ε are turbulence Prandtl numbers for k and ε, respectively. G_k and Y_k denote production and dissipation terms for k, while G_ε and Y_ε are production and dissipation terms for ε. Single step mechanism is invoked to model chemical reactions. For instance, the methane-air reaction mechanism is expressed as:

$$CH_4 + 2O_2 + 7.52N_2 \longrightarrow CO_2 + 2H_2O + 7.52N_2 \tag{14}$$

The gas mixture consists of 5 chemical species. The liquid fuels are assumed to be pre-vaporized. In a real combustor, turbulence plays a key role in fuel-air mixing and reaction process. In the current study eddy dissipation model (EDM) (Magnussen and Hjertager 1977; Spalding 1971) is employed to calculate the overall reaction rate. The EDM have a high computational speed, and yet it provides satisfactory accuracy for mixing-limited diffusion flames. In this model, the net rate of production of i'th species is obtained by the smaller term of the two following expressions:

$$\dot{\omega}_i = v_i' M_i A \rho \frac{\varepsilon}{k} \min\left(\frac{Y_R}{v_R' M_R}\right) \tag{15}$$

$$\dot{\omega}_i = v_i' M_i A B \rho \frac{\varepsilon}{k} \frac{\sum_P Y_P}{\sum_j^N v_j'' M_j} \tag{16}$$

In the above equations, v' and v'' represent the stoichiometric coefficients for reactants and products, respectively; M denotes the molecular weight and ρ is the density. The subscripts R and P represent reactants and products. A=4.0 and B=0.5 are the empirical constants. The final reaction rate is the smaller rate calculated by the preceding two equations.

Simulations are carried out using ANSYS FLUENT v19.0. A steady two-dimensional pressure-based solver is employed to simulate reacting flow in the nozzle. Conservation equations are discretized using second-order upwind scheme. Thermophysical properties are considered to be temperature and species dependent. Ideal gas mixing law is invoked to calculate constant-pressure specific heat, conductivity and viscosity of

the gas mixture. The constant-pressure specific heat for each chemical species is obtained by a piecewise polynomial function of temperature. Molecular viscosity for each species is calculated by Sutherland law, while conductivity of each species is assumed to be constant. The convergence criterion was set to be a residual error of 10^{-5} for all equations. Simulations are performed using a computer with 8 CPU cores and each simulation took 10 hours to finish.

A pressure-inlet boundary condition is considered for the primary inlet at which the static pressure is determined by the nozzle NPR (which is fixed at NPR=4 in the present study), while the mass flow rate is specified for the secondary inflow. The mass flow rate of secondary flow is established based on the required side-injection percentage from total mass flow rate. Temperatures at both inlets are fixed at $300\ K$. Turbulence intensity is set to 10% at both inlets. A pressure-outlet boundary condition is imposed at the outlets with a pressure equal to 1 atm. The walls are considered to be no-slip, adiabatic and impenetrable.

3. NOZZLE PERFORMANCE PARAMETERS

In order to evaluate the nozzle performance, different parameters and criterions are proposed, such as discharge coefficient, thrust ratio, thrust-vector angle, thrust-vectoring efficiency and thrust loss percentage (Hamedi *et al.* 2015; Flamm *et al.* 2006). Another criterion is employed in the current study, which is defined as the ratio of thrust to total mass flow rate passing the nozzle. The mentioned criterions are briefly defined in the following. Discharge coefficient (C_d) is defined as the ratio of actual mass flow rate of nozzle to ideal isentropic flow rate:

$$C_d = \frac{w_p + w_s}{w_{ip}} \tag{17}$$

$$w_{ip} = \frac{P_0 A_{throat}}{\sqrt{RT_0}} \sqrt{\gamma} \left(\frac{2}{\gamma+1}\right)^{\frac{\gamma+1}{2(\gamma-1)}} \tag{18}$$

Where w_p and w_s denote actual primary and secondary inlet mass flow rates of nozzle while w_{ip} stands for ideal primary inlet mass flow rate. $\gamma = 1.4$ is specific heats ratio, $R = 287.3\ J/kg.K$ is air gas constant and P_0 and T_0 denote stagnation pressure and temperature at the primary inlet. Thrust ratio (C_f) is defined as the ratio of actual resultant thrust of nozzle to ideal isentropic thrust:

$$C_f = \frac{F_r}{F_{ip} + F_{is}} \tag{19}$$

$$F_{ip} + F_{is} = (w_p + w_s)\sqrt{RT_0\left(\frac{2\gamma}{\gamma-1}\right)\left[1-\left(\frac{P_{ambient}}{P_0}\right)^{\frac{\gamma-1}{\gamma}}\right]} \tag{20}$$

Where F_{ip} and F_{is} denote ideal isentropic thrusts of primary and secondary flows, respectively, while $F_r = \sqrt{F_a^2 + F_n^2}$ is the resultant actual thrust. F_a is axial thrust and F_n is normal thrust. $P_{ambient} = 101\ kPa$ is ambient pressure. Thrust-vector angle (δ_p) is defined as the deflection angle of thrust vector relative to axial direction, which is calculated as:

$$\delta_p = tan^{-1}\left(\frac{F_n}{F_a}\right) \tag{21}$$

Thrust-vectoring efficiency (η) is expressed as the ratio of thrust-vector angle to secondary injection percentage from total mass flow rate (ϕ):

$$\eta = \frac{\delta_p}{\phi}\ (deg/\%) \tag{22}$$

$$\phi = \frac{w_s}{w_s + w_p} \times 100\% \tag{23}$$

Therefore, vectoring efficiency actually is the vector angle for 1% secondary injection and it's unit is degrees per percent secondary injection. Another criterion employed in the present study is thrust loss percentage relative to a similar case with no secondary injection. A nozzle with lower thrust loss percentage would be more desirable. The last parameter is the ratio of thrust to total mass flow rate ($F_r/(w_s + w_p)$). This parameter indicates the thrust value for 1 kg/s flow rate passing the nozzle.

4. VALIDATION

In this section, simulations of supersonic flow inside a thrust-vectoring DTN are performed to validate the numerical methods employed in the present study. The numerical results are compared with the experimental data acquired in the Flamm *et al.* (2005) study. Their experiments include measurements of thrust-vectoring parameters for a 3D non-reacting supersonic planar DTN. The geometry and boundary conditions in the experiments of Flamm *et al.* (2005) are shown in the Fig. 1 and can be found with more details in their study.

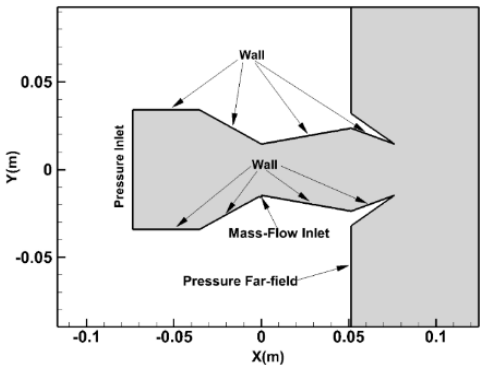

Fig. 1. Sketch illustrating the geometry of Dual Throat Thrust Vectoring Nozzle in the Flamm *et al.* (2006) experiment.

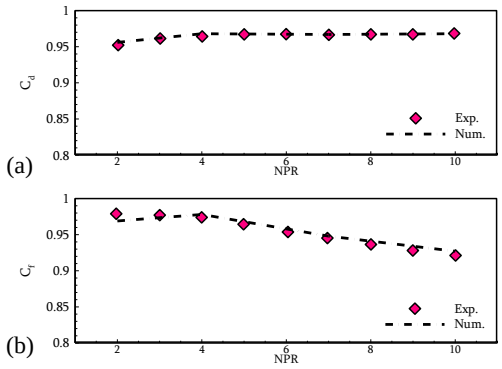

Fig. 2. Variation of (a) nozzle discharge coefficient and (b) thrust ratio, with nozzle pressure ratio (NPR) for cavity length 1.0" and no secondary injection. Dash-dot lines: Numerical results; Symbols: experiments of Flamm *et al*. (2006).

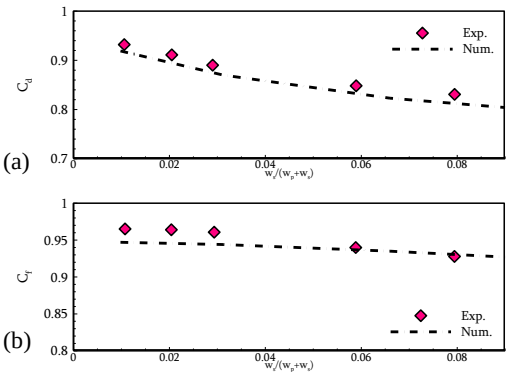

Fig. 3. Variation of (a) nozzle discharge coefficient and (b) thrust ratio, with secondary injection rate for cavity length 2.0" and NPR=4. Dash-dot lines: Numerical results; Symbols: experiments Flamm *et al*. (2006).

They have measured discharge coefficient, thrust ratio, vectoring angle, vectoring efficiency and wall pressure distribution in terms of NPR, secondary injection rate and cavity length. In the current study, their experiments have been simulated and the mentioned parameters have been calculated and compared to their experimental counterparts. The secondary injection angle with horizontal direction is fixed at 150 degrees.

Figure 2 shows variations of discharge coefficient and thrust ratio with NPR when the cavity length is 1.0 inch and no secondary injection is existing. The curves demonstrate a very good consistency with experimental data for all considered NPR's. Fig. 3 shows variations of discharge coefficient and thrust ratio with secondary injection rate when the cavity length is 2.0 inches and NPR is 4.0. This curves also depict a very good consistency with experimental data for the considered injection rate range. So far, the numerical scheme is very efficient in predicting nozzle discharge coefficient and thrust ratio in typical ranges of NPR and side-injection rate.

Figure 4 depicts variations of vectoring angle and vectoring efficiency with side-injection rate for a DTN with cavity length of 1.0 inch and NPR of 4. This curves also exhibits the capability of numerical scheme for estimating the deflection quantities of the nozzle.

The distribution of normalized static pressure along upper and lower walls of a DTN with cavity length of 2.5" and NPR=4, is shown in the Fig. 5. There are two minimums at the throat positions i.e. x/L=0 and x/L=1, which could be the direct consequence of maximizing the velocity at throats. Also, a good consistency is observable between numerical and experimental results.

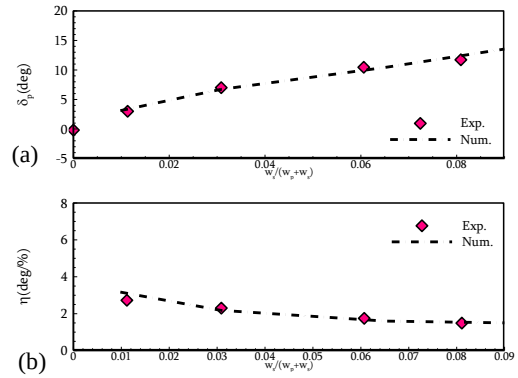

Fig. 4. Variation of (a) thrust-vector angle and (b) thrust-vectoring efficiency, with secondary injection rate for cavity length 1.0" and NPR=4. Dash-dot lines: Numerical results; Symbols: experiments of Flamm *et al*. (2006).

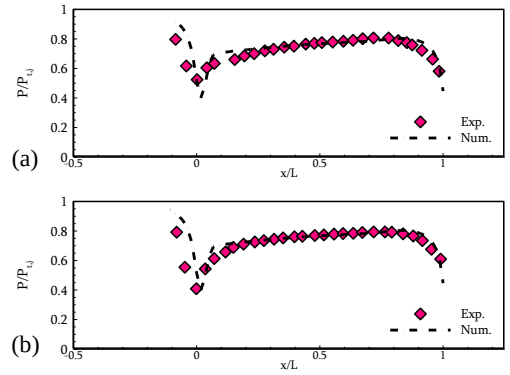

Fig. 5. Normalized pressure distribution on (a) Upper surface and (b) Lower surface of the DTN with cavity length 2.5" and NPR=4 and no secondary injection. Dash-dot lines: Numerical results; Symbols: experiments of Flamm *et al*. (2006).

5. COMPUTATIONAL GEOMETRY AND GRID

The DTN geometry in the current study is a 3D thrust-vectoring geometry similar to the validation cases, which is shown with details in the Fig. 6(a). The cavity length and side-injection angle are fixed at $l = 3.0\ in$ and $\alpha = 150°$, respectively. These

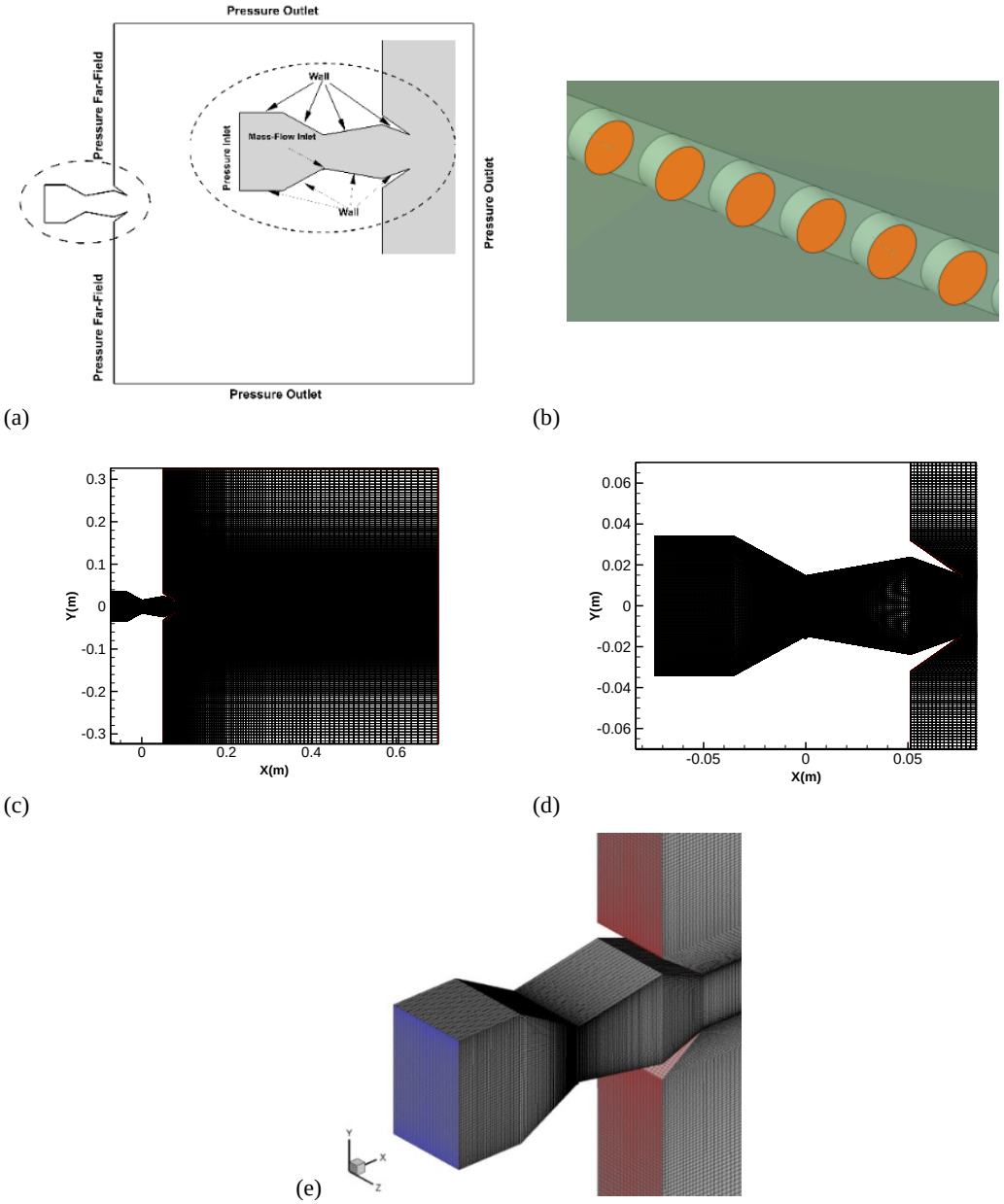

Fig. 6. (a) Simulation domain for the considered DTN; (b) geometry of circular injectors; (c) reference grid for the entire domain, (d) reference grid for the nozzle, (e) 3D reference grid for the nozzle.

parameters are selected based on best performance in terms of vectoring angle and efficiency, which is reported in the Flamm *et al.* (2005) study. Moreover, the nozzle pressure ratio is kept constant at NPR=4. The injection is carried out using two types of injection geometry with equivalent open areas: (1) a slot injector which covers the whole span of nozzle with the slot width of 0.0216", (2) a row of circular injectors with diameter of 0.05". The center to center distance of circular injectors is variable from 0.09" to 0.27" which will be explained in the next sections. The geometry of circular injectors with the center to center distance of 0.09" is depicted in the Fig. 6(b). The 3D structured computational grid is generated using ANSYS Meshing v19.0. 2D and 3D views of the grid are displayed in the Fig. 6(c-e). The grid is clustered in the high gradient regions. The first cell layer adjacent to the walls is selected such that $y^+$is around unity.

The quality of employed mesh is evaluated through a mesh independence study, which is performed among four different grid resolutions. The number of cells for these grids is presented in the Table 1.

Table 1. Details of four different grids

	Coarse	Medium	Fine	Very Fine
Number of cells	500K	800K	1.5M	2.5M

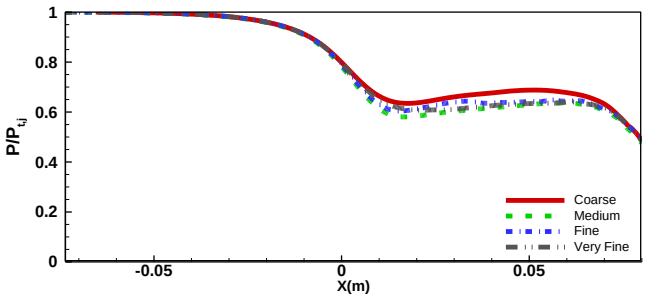

Fig. 7. Normalized pressure distribution on the nozzle center-line for different grid resolutions.

Figure 7 shows normalized static pressure along the nozzle center-line for all four grids. The result derived from the coarse grid demonstrates a certain deviation from the other three grids, whereas the static pressure curve of medium, fine and very fine grids are very close. Therefore, the medium grid resolution is chosen as the reference grid to perform the rest of the simulations.

6. RESULTS AND DISCUSSION

6.1. Effects of Secondary Injection Rate

In this section, slot injection of methane is simulated and examined so as to describe physicals phenomena occurring in thrust-vectoring process of reacting DTN's. To do this, distributions of fuel mass fraction, velocity magnitude, static pressure, Mach number and temperature are invoked and scrutinized. All distributions and contours in the current study are presented on the nozzle center-plane shown in the Fig. 6(b). Two-dimensional streamlines along with fuel mass fraction distributions for different injection rates are presented in the Fig. 8. It can be observed that in the case without secondary injection ($\phi = 0$), a recirculation zone (RZ) is created inside each one of upper and lower cavities which are of equal size. In other words, the main jet is symmetric and there is no flow vectoring. With 1% secondary injection, the lower RZ grows and the upper RZ shrinks. This is caused by the creation of a separation flow region in the lower cavity due to secondary injection, which deflects the main flow and establishes flow vectoring. By increasing the injection rate to $\phi =$ 3%, the lower RZ grows further and the upper RZ vanishes, which leads to enhancement of main jet vectoring. With further increment of injection rate, additional enlargement of lower cavity RZ can be observed which assists the deflection of the main jet and flow vectoring.

In order to gain more insight about the flowfield of DTN, the velocity magnitude distributions for different injection rates are displayed in the Fig. 9. The figures suggest that for cases with injection, a high-speed layer is created in the lower region of the jet coming out of the nozzle. This layer which is pointed by arrowhead, have a velocity nearly twice as large as nozzle outlet. It is originated from the fuel reaction which leads to volume expansion and

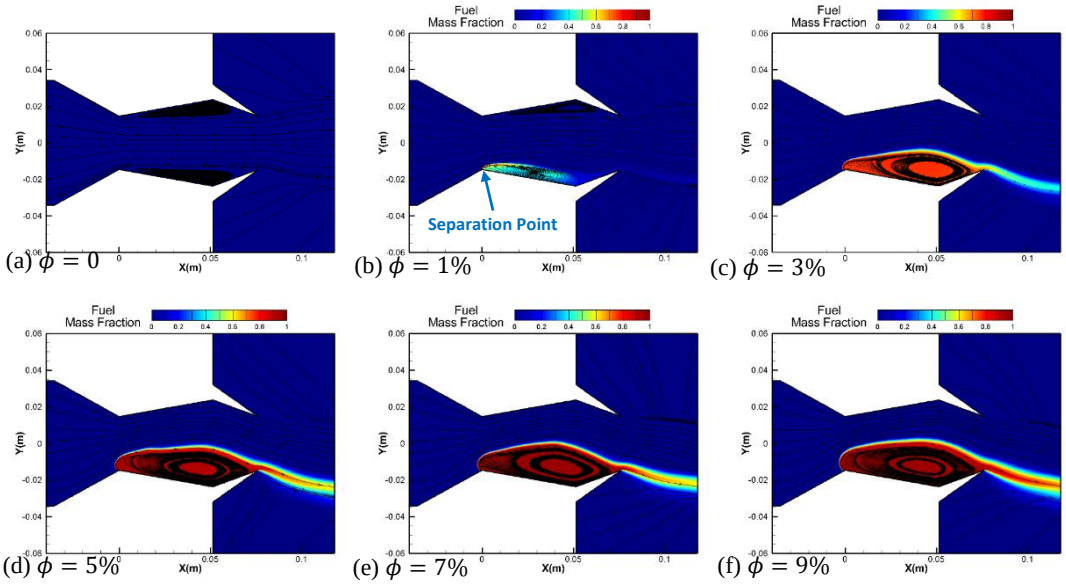

Fig. 8. Distributions of fuel mass fraction along with 2D streamlines for slot injection of methane.

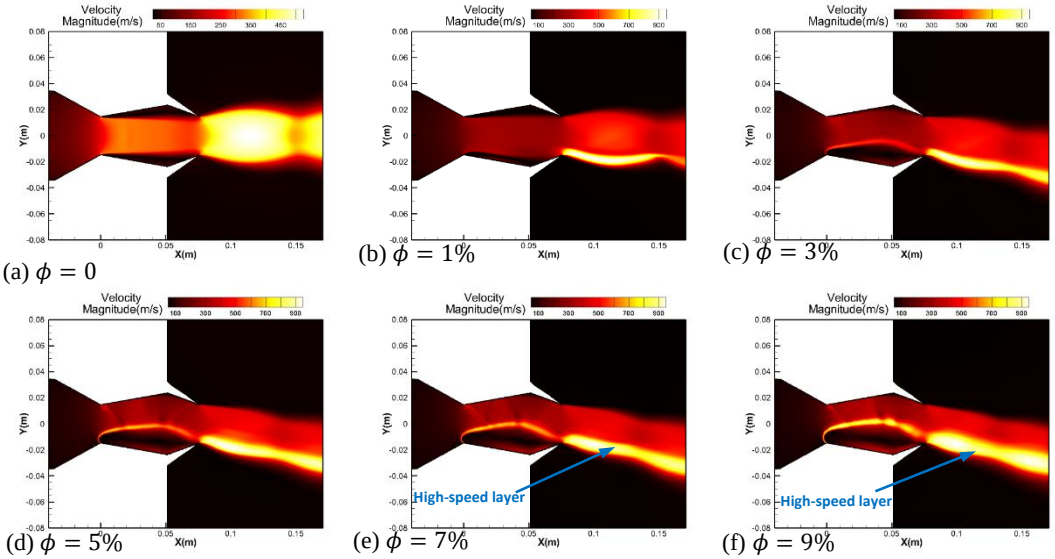

Fig. 9. Distributions of velocity magnitude for slot injection of methane.

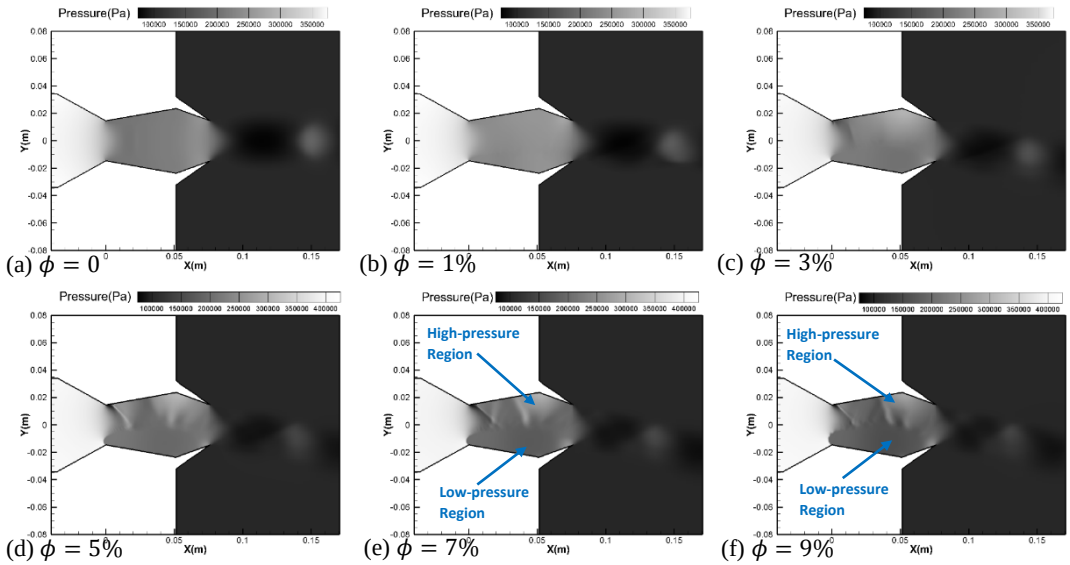

Fig. 10. Distributions of static pressure for slot injection of methane.

s

acceleration of the jet in the lower region of outlet. As a result, thrust could be dramatically amplified, which will be verified in the next section.

As mentioned earlier, pressure difference between upper and lower cavities enhances vectoring in DTN's. In this section, pressure distributions are invoked to examine the issue. Fig. 10 shows static pressure contours for all injection rates. As expected, the distribution is symmetric for non-injection case. The symmetry vanishes with increasing the injection rate. A low-pressure RZ is created in the lower cavity due to flow separation, whereas, the upper cavity is filled with a high-speed high-pressure flow. Pressure asymmetry assists vectoring in DTN's.

In order to provide a visual perception of flow vectoring, distributions of Mach number for different injection rates are presented in the Fig. 11. Direction of the flow exiting the nozzle is represented by a black vector. It can be observed that, the vector angle with horizon line grows by increasing the injection rate and vectoring is achieved. More details for flow vectoring will be provided in the next section.

In order to shed light on fuel combustion effects, temperature distribution for all injection rates are invoked. As can be seen in Fig. 12, a hot mixing layer is established at the interface between main jet flow and lower cavity RZ, which is direct consequence of reaction of fuel and air in this layer. Moreover, a hot RZ is formed inside the lower cavity due to accumulation of hot combustion products. This region has a high specific volume due to high temperatures and resulting volume expansion. Thereby, could potentially enhance flow vectoring. The impacts of high specific volume on the vectoring will be quantitatively examined in the next section.

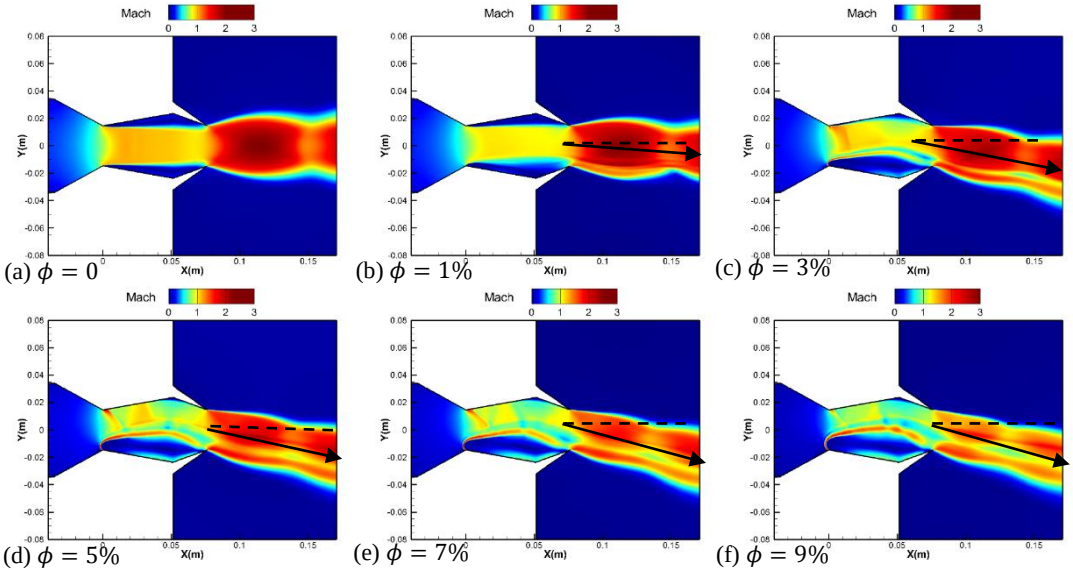

Fig. 11. Distributions of Mach number for slot injection of methane.

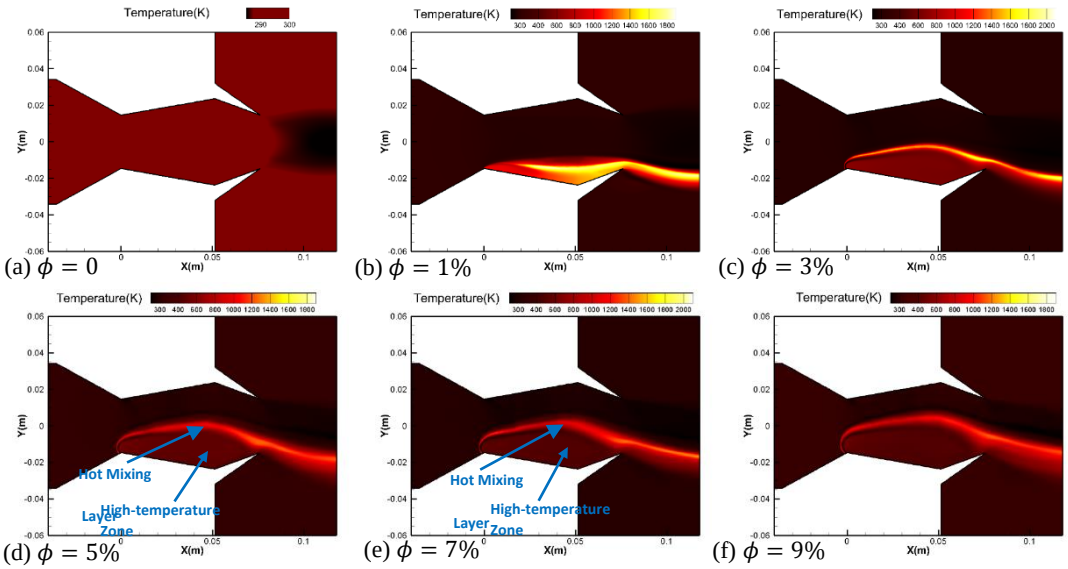

Fig. 12. Distributions of temperature for slot injection of methane.

A three-dimensional distribution of fuel mass fraction along with 3D streamlines for slot injection of methane at $\phi = 7\%$ are depicted in the Fig. 13. The distribution gives a better perception of role of fuel side-injection in deflecting the main flow.

6.2. The Effects of Injection Geometry

In this section the impact of geometry of injection ports on nozzle thrust-vectoring performance is evaluated. Two different geometries with equivalent open areas are considered for injectors: (1) a slot which is 0.0216" wide and extended in the spanwise direction, and (2) a row of circular holes each having a diameter of 0.05" with a fixed center-to-center space of 0.09". Also, four different fuels are injected including methane, propane, octane and kerosene. All mentioned nozzle performance parameters are extracted and reported. Fig. 14 shows the secondary-to-primary momentum flux ratio $MFR = \rho_s V_s^2 / \rho_p V_p^2$ for different fuels injected through slot and circular injectors. It can be seen that the momentum ratios are equivalent for two injection geometries of each fuel due to equivalency of injection areas. Heavier fuels obviously have lower momentum ratios due to higher density. Fig. 15 presents the nozzle discharge coefficient for two injection geometries and different fuels. Slot injection provide higher discharge coefficient for all considered fuels.

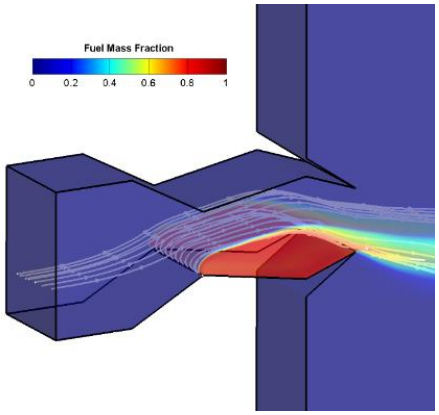

Fig. 13. 3D distribution of fuel mass fraction along with 3D streamlines for slot injection of methane.

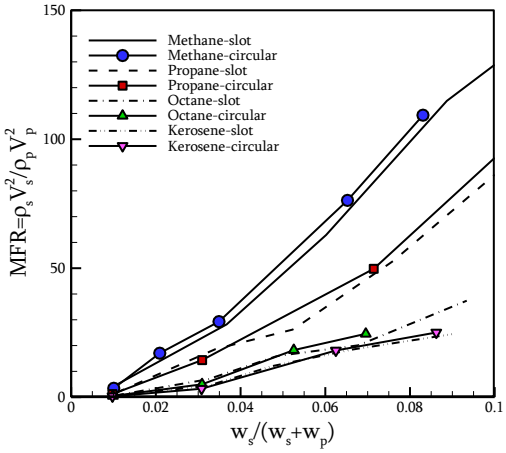

Fig. 14. Variation of secondary-to-primary momentum flux ratio (MFR) with secondary injection rate for slot and circular injection of different fuels.

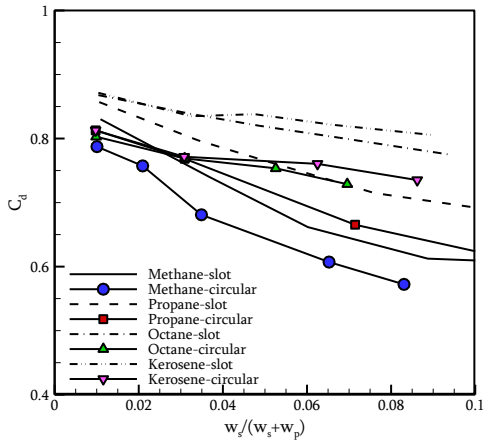

Fig. 15. Variation of discharge coefficient with secondary injection rate for slot and circular injection of different fuels.

That means employing slot injector causes that higher mass flow to pass through the nozzle. Heavier fuels have greater discharge coefficient due to lower injection momentum.

Figure 16 presents the nozzle thrust ratio for two injection geometries. Values higher than unity are obtained for thrust ratio. The reason is the remarkable increase in thrust due to combustion inside and outside the nozzle, which makes the resultant actual thrust to surpass the ideal isentropic thrust. It can be observed that circular injectors cause higher thrust ratio for all considered fuels. Slot injector provides a continuous injection, while circular injectors establish relatively discrete injection. The side-injection inevitably leaves reducing effects on thrust, thus employing circular injectors instead of slot injector, breaks the injection continuity and thereby mitigates the reducing effects on thrust. Unlike discharge coefficient, thrust ratio is higher for lighter fuels.

Thrust-vector angle and vectoring efficiency are invoked as a measure of mainstream deflection at the nozzle outlet. Table 2 is a collection a data for thrust-vector angle at different secondary injection rates (ϕ) for slot and circular injection of different fuels.

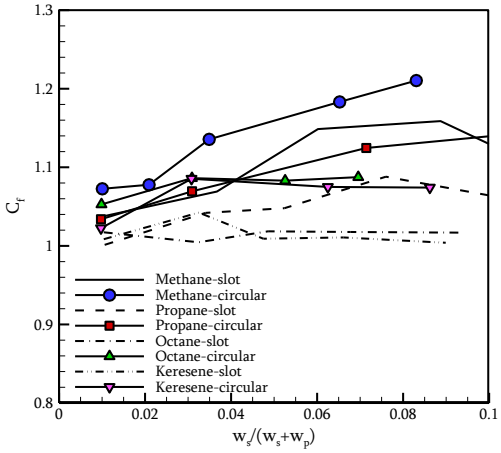

Fig. 16. Variation of thrust ratio with secondary injection rate for slot and circular injection of different fuels.

Moreover, Fig. 17. presents the thrust vector angle and vectoring efficiency for two injection geometries and different fuels. Also, in order to make a comparison and better understand the effects of fuel reaction, experimental observations of Flamm *et al.* (2006) for a similar nozzle and injection geometry but with inert injectant (air) are presented. Maximum secured vectoring angle is 17.1 degrees with slot injection of methane fuel at 9% injection rate. As observed, slot injector provides higher vectoring angle and efficiency for all mentioned fuels. At $\phi = 2\%$ for methane fuel, vectoring angle and vectoring efficiency for slot injector is 8% and 34% greater than those obtained by circular injector, respectively. This can be attributed to the continuity of injection. Employing slot injector creates a continuous injection while circular injection have a less continuous (or even discrete) injection. Therefore, slot injector has a higher ability to deflect the main jet, so, the deflection is fortified and also vectoring angle and

Table 2. Values of thrust-vector angle ($\delta_p(deg)$) at different secondary injection rates (ϕ) for slot and circular injection of different fuels

Fuel-Geometry	ϕ				
	1%	3%	5%	7%	9%
Methane-slot	9.5	13.2	15.8	17.0	17.1
Methane-circular	9	10.1	12.8	15.3	16.5
Propane-slot	3.9	8.1	9.5	11.4	15.1
Propane-circular	3.6	4.7	--	7.3	9
Octane-slot	3.2	5.8	7.7	9	10.4
Octane-circular	3.6	3.8	4.4	5	--
Kerosene-slot	2.9	5	6.8	8.1	9.3
Kerosene-circular	3.1	3.6	--	4.3	5
Air-slot (Flamm *et al*. (2006))	7.7	12.7	---	13	11.4
Air-circular (Flamm *et al*. (2006))	6.4	11.9	---	14.8	15.3

efficiency. Comparing methane results of slot and circular injectors with their experimental inert counterparts conducted by Flamm *et al*. (2006), reveals that injecting methane produces higher vectoring angle and efficiency for both injection geometries, however injecting other fuels doesn't provide such improvements. Specifically, at the injection rate of $\phi = 8\%$, vectoring angle of slot injector for methane is 16.7 degrees while for air is 11.4 degrees. At the same rate, vectoring angle of circular injector for methane is 16.3 degrees while for air is 15.3 degrees. In the other words, employing methane instead of air, improves vectoring angle by 46% for slot injector and by 7% for circular injector. The same trend is true for vectoring efficiency. At the injection rate of $\phi = 8\%$, employing methane instead of air, improves vectoring efficiency by 53% for slot injector and by 9% for circular injector. This improvements in vectoring angle and efficiency of methane injection can be attributed to the volume expansion caused by reaction and the resulting temperature rise in the cavity zone. Volume expansion in the lower cavity pushes the main jet upward and enhances the jet deflection. Light fuels generate higher vectoring angles and efficiency due to higher secondary-to-primary momentum ratio.

Figure 18. presents the nozzle thrust-to-mass-flow ratio for two injection geometries and different fuels. As mentioned in the above, circular injectors provide higher thrust ratio than slot injector. Thereby, it is expected that thrust to mass flow ratio would be higher for circular ports. This is also true for lighter fuels which create higher thrust than heavier fuels. The collected data for thrust-to-mass-flow ratio at different secondary injection rates for slot and circular injection of different fuels are provided in the Table 3.

6.3. The Effects of Center-To-Center Distance of Injector Holes

It was proved in the previous section that slot injection provides better vectoring and is preferable to circular injection. However, due to easier manufacturing, circular injectors still have been popular so far. Therefore, it is beneficial to study circular injection with more details. In this section we assume that the side-injection is performed using circular injectors. With this presumption, the impact of center-to-center distance of side-injection holes (L_p) on the performance is examined. Three distances of 0.09", 0.18" and 0.27" is considered, while only methane injection is simulated due to advantages proved in the previous section. All previously mentioned performance parameters are

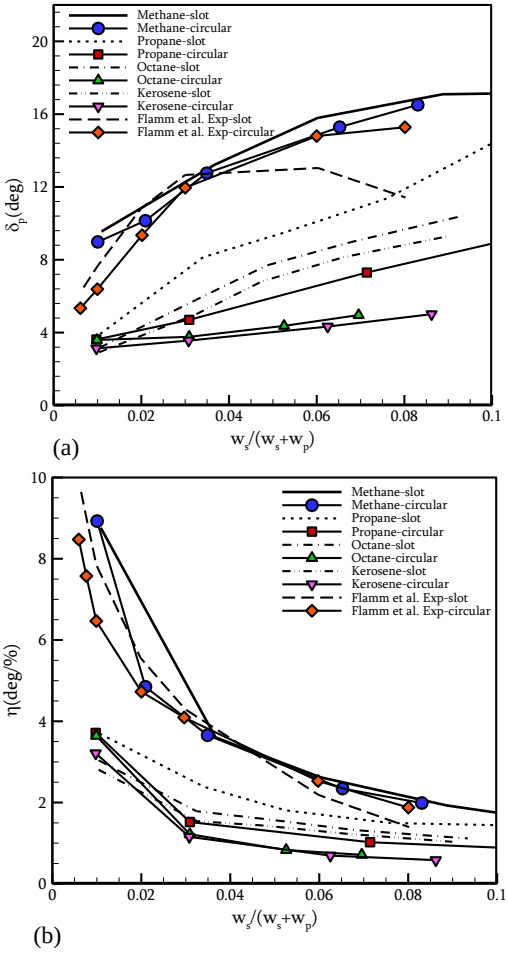

Fig. 17. Variation of (a) thrust-vector angle and (b) thrust-vectoring efficiency, with secondary injection rate for slot and circular injection of different fuels.

Table 3. Values of thrust-to-mass-flow ratio (F_r⁄(w_s+w_p)((N.s)⁄kg)) at different secondary injection rates (ϕ) for slot and circular injection of different fuels

Fuel-Geometry	ϕ				
	1%	**3**%	**5**%	**7**%	**9**%
Methane-slot	461	475	510	515	479
Methane-circular	476	479	504	526	538
Propane-slot	445	463	465	483	470
Propane-circular	459	475	--	500	507
Octane-slot	452	446	452	452	452
Octane-circular	468	482	---	481	483
Kerosene-slot	448	463	448	449	446
Kerosene-circular	454	482	--	478	477

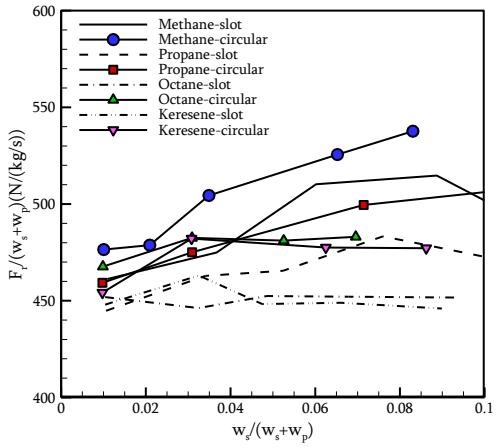

Fig. 18. Variation of thrust to mass flow ratio with secondary injection rate for slot and circular injection of different fuels.

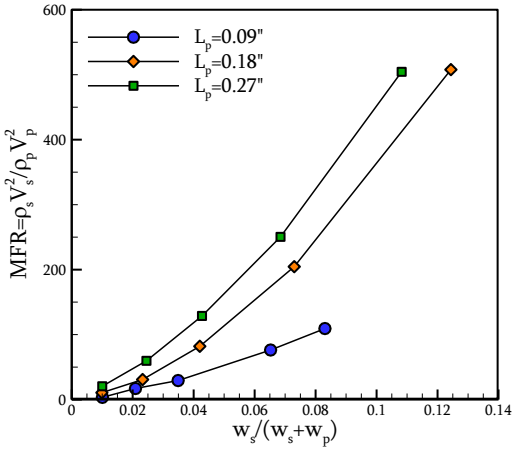

Fig. 19. Effect of center-to-center distance of injector holes (L_p) on secondary-to-primary momentum flux ratio (MFR) for circular injection of methane.

extracted from the simulations and reported in the following. Fig. 19 shows the secondary-to-primary momentum flux ratio (MFR) for the considered L_p's. We can see that increasing L_p boosts MFR. That's because with increasing L_p, the overall injection area is reduced and the side-injection velocity inevitably increases.

Figure 20. depicts variations of nozzle discharge coefficient with secondary injection rate. It can be observed that with increasing L_p, discharge coefficient is reduced. This can be attributed to the increasing of MFR. With growing MFR, the secondary flow enters the nozzle with higher momentum and establishes a stronger obstruction in the primary flow.

Figure 21. depicts variations of nozzle thrust ratio with secondary injection rate. All values are more than one, which its reason was explained in the previous section. It can be seen that with increasing L_p, thrust ratio increases, i.e. the resultant thrust increses. The reason for this is explained in the following.

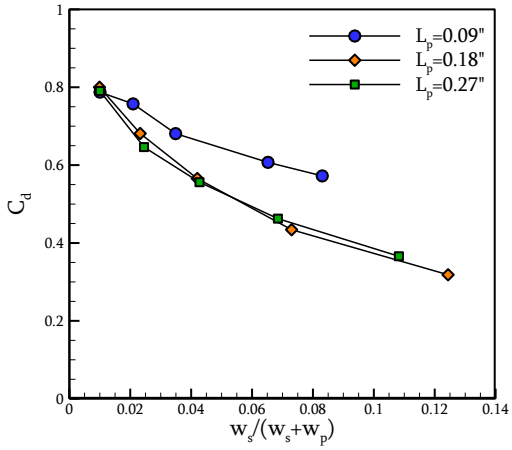

Fig. 20. Effect of center-to-center distance of injector holes (L_p) on discharge coefficient for circular injection of methane.

Figure 22. shows variations of nozzle vectoring angle and thrust-vectoring efficiency with secondary injection rate. Moreover, Table 3 presents the data for thrust-vector angle at different center-to-center distances (L_p) for circular injection of methane. It can be observed that increasing L_p, decreases both vectoring angle and efficiency. To be more precise, at the side-injection rate of $\phi = 8\%$, increasing L_p from 0.09" to 0.27", decreases vectoring angle by 50% and vectoring efficiency by 48%. That's

Table 3. Values of thrust-vector angle ($\delta_p(deg)$) at different center-to-center distances (L_p) for circular injection of methane

$L_p(inches)$	ϕ				
	1%	**3%**	**4%**	**7%**	**9%**
0.09	9	10.1	12.8	15.3	16.5
0.18	9	10.1	10.4	9.2	8
0.27	7.2	8.0	8.8	8.6	7.6

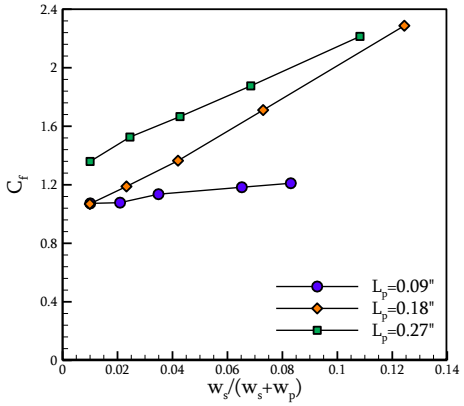

Fig. 21. Effect of center-to-center distance of injector holes (L_p) on thrust ratio for circular injection of methane.

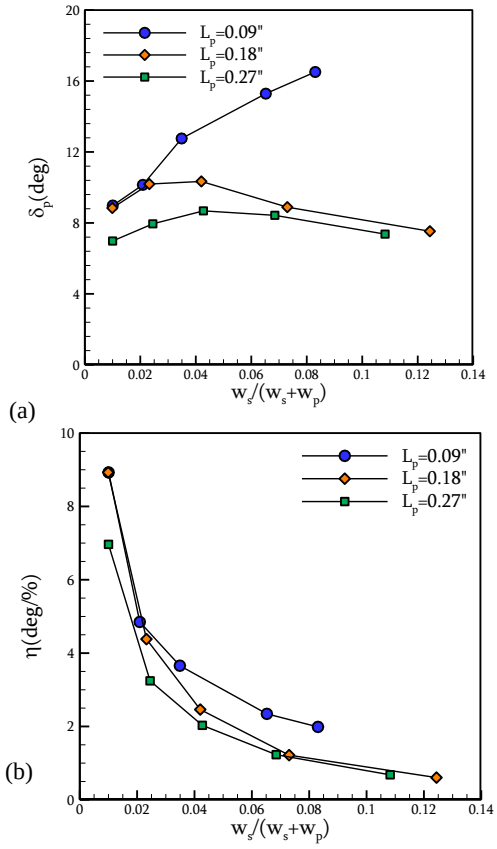

Fig. 22. Effect of center-to-center distance of injector holes (L_p) on (a) thrust-vector angle and (b) thrust-vectoring efficiency, for circular injection of methane

because increasing L_p, makes the injection more discrete and separated and thus, impairs the secondary jets ability to deflect the main jet. Thereby, the deflection is weakened and also vectoring angle and efficiency.

Figure 23. shows variations of thrust to mass flow ratio with secondary injection rate. Increasing L_p, leads to an increase in thrust to mass flow ratio, i.e. the more distant holes are, the higher resultant thrust nozzle produces. The secondary jets inevitably have reducing effects on thrust, thus increasing their distance escalates injectors detachment and thereby impairs the reducing effects on thrust. That's the reason why thrust ratio (Fig. 21) and thrust to mass flow ratio (Fig. 23) experience an improvement with increasing L_p. Fig. 24 shows variations of thrust loss percentage with secondary injection rate. As expected, a higher L_p, results in a higher thrust and thereby a lower thrust loss relative to non-injecting case.

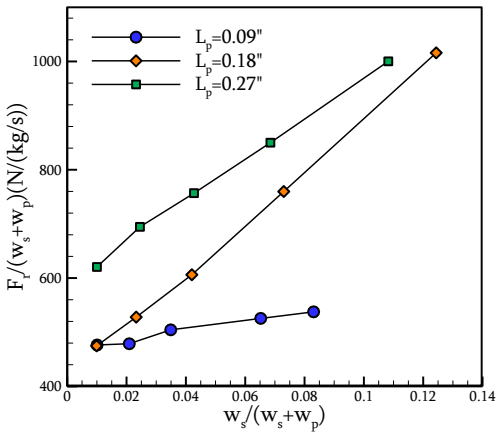

Fig. 23. Effect of center-to-center distance of injector holes (L_p) on thrust to mass flow ratio for circular injection of methane.

1. CONCLUSION

Numerical investigation of fluidic dual throat thrust-vectoring nozzle with fuel side-injection is carried out. Favre-averaged momentum, energy and species equations are solved and standard $k-\varepsilon$ model along with eddy-dissipation model are invoked to close turbulence and combustion interactions. Different parameters are employed to assess thrust-vectoring performance of the nozzle such as discharge coefficient, thrust ratio, thrust-vector angle and thrust-vectoring efficiency. The numerical

results are compared well with the existing experimental measurements. The impacts of the geometry of injector cross-section as well as center-to-center distance of injector holes on the thrust-vectoring performance of the nozzle is studied. Two geometries are considered as injector cross-section: slot and circular, while four different fuel injectants are employed. The results have suggested the following conclusions:

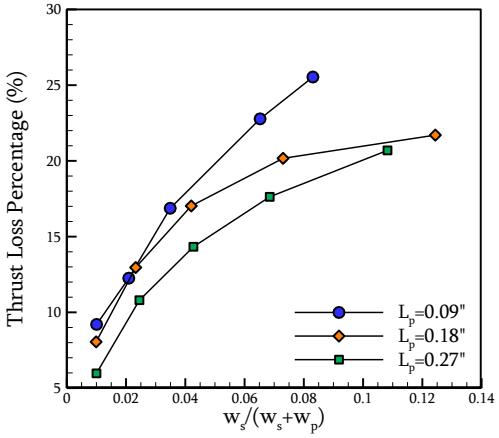

Fig. 24. Effect of center-to-center distance of injector holes (L_p) on thrust loss for circular injection of methane.

- Overall, a maximum vector angle of 17.1 degrees is achieved via slot injection of methane at a secondary injection rate equal to 9% of primary flow rate.
- Investigating the effects of geometry of injector cross-section reveals that slot injection provides a stronger performance in terms of discharge coefficient, vector angle and vectoring efficiency, whereas circular injection have a better thrust ratio and thrust to mass flow ratio for all considered fuels. At 2% injection for methane, vector angle and vectoring efficiency obtained by slot injector is 8% and 34% higher than the circular injector, respectively.
- Investigating the effects of fuel type shows that heavy fuels have a better discharge coefficient, however light fuels generate a higher thrust ratio, thrust to mass flow ratio, vector angle and vectoring efficiency.
- Investigating the impact of center-to-center distance of injector holes reveals that higher distances offer higher thrust ratios, while having lower discharge coefficient, vector angle and vectoring efficiency. At the injection rate of 8% for methane, increasing center-to-center distance from 0.09" to 0.27", decreases vectoring angle by 50% and vectoring efficiency by 48%.
- In general, in order to achieve a higher vector angle and vectoring efficiency, slot injection of methane is recommended.
- Comparing inert and reactive injectants shows that employing methane fuel instead of inert injectants, crucially improves vectoring performance.
- Secondary-to-primary momentum flux ratio is demonstrated to have substantial effects on nozzle performance.

REFERENCES

Anderson, C., V. Giuliano, D. C. Wing (1997). Investigation of Hybrid Fluidic/Mechanical Thrust Vectoring for Fixed-Exit Exhaust Nozzles. *In 33rd Joint Propulsion Conference and Exhibit*, 3148.

Aleiferis, P. G. and N. Papadopoulos (2021). Heat and mass transfer effects in the nozzle of a fuel injector from the start of needle lift to after the end of injection in the presence of fuel dribble and air entrainment. *International Journal of Heat and Mass Transfer* 165, 120576.

Berni, F., G. Cicalese, M. Borghi and S. Fontanesi (2021). Towards grid-independent 3D-CFD wall-function-based heat transfer models for complex industrial flows with focus on in-cylinder simulations. *Applied Thermal Engineering* 190, 116838.

Bordoloi, N., K. M. Pandey and K. K. Sharma, (2021). Numerical Investigation on the Effect of Inflow Mach Numbers on the Combustion Characteristics of a Typical Cavity-Based Supersonic Combustor. *Mathematical Problems in Engineering*, 2021.

Chen, S., S. M. Randy Chue, C. M. Simon Yu and J. U. Schlüter (2016). Spinning Effects on a Trapped Vortex Combustor. *Journal of Propulsion and Power* 32 (5), 1133–1145.

Deere, K. (1998) PAB3D Simulations of a Nozzle with Fluidic Injection for Yaw Thrust-Vector Control." In *34th AIAA/ASME/SAE/ASEE Joint Propulsion Conference and Exhibit*, 3254.

Deere, K. (2000). Computational Investigation of the Aerodynamic Effects on Fluidic Thrust Vectoring. In *36th AIAA/ASME/SAE/ASEE Joint Propulsion Conference and Exhibit*, 3598.

Deere, K. (2003). Summary of Fluidic Thrust Vectoring Research at NASA Langley Research Center. In *21st AIAA Applied Aerodynamics Conference*, 3800.

Deere, K., B. Berrier, J. Flamm and S. Johnson (2003). Computational Study of Fluidic Thrust Vectoring Using Separation Control in a Nozzle. In *21st AIAA Applied Aerodynamics Conference*, 3803.

Deere, K., B. Berrier, J. Flamm and . Johnson

(2005). A Computational Study of a Dual Throat Fluidic Thrust Vectoring Nozzle Concept. In *41st AIAA/ASME/SAE/ASEE Joint Propulsion Conference & Exhibit*, 3502.

Deere, K., J. Flamm, B. Berrier and S. Johnson (2007). Computational Study of an Axisymmetric Dual Throat Fluidic Thrust Vectoring Nozzle for a Supersonic Aircraft Application. In *43rd AIAA/ASME/SAE/ASEE Joint Propulsion Conference & Exhibit*, 5085.

Federspiel, J., L. Bangert, D. Wing and T. Hawkes (1995). Fluidic Control of Nozzle Flow-Some Performance Measurements. In *31st Joint Propulsion Conference and Exhibit*, 2605.

Flamm, J. (1998). Experimental Study of a Nozzle Using Fluidic Counterflow for Thrust Vectoring. In *34th AIAA/ASME/SAE/ASEE Joint Propulsion Conference and Exhibit*, 3255.

Flamm, J., K, Deere, B, Berrier, S, Johnson and M. Mason (2005). Experimental Study of a Dual-Throat Fluidic Thrust-Vectoring Nozzle Concept. In *41st AIAA/ASME/SAE/ASEE Joint Propulsion Conference & Exhibit*, 3503.

Flamm, J., K. Deere, M. Mason, B. Berrier and S. Johnson (2006). Design Enhancements of the Two-Dimensional, Dual Throat Fluidic Thrust Vectoring Nozzle Concept. In *3rd AIAA Flow Control Conference*, 3701.

Flamm, J., K. Deere, M. Mason, B. Berrier and S. Johnson. (2007). Experimental Study of an Axisymmetric Dual Throat Fluidic Thrust Vectoring Nozzle for Supersonic Aircraft Application. In *43rd AIAA/ASME/SAE/ASEE Joint Propulsion Conference & Exhibit*, 5084.

Forghany, F, M. Taeibe-Rahni and A Asadollahi-Ghohieh (2017). Numerical Investigation of Optimization of Injection Angle Effects on Fluidic Thrust Vectoring. *Journal of Applied Fluid Mechanics* 10 (1), 157–167.

Giuliano, V., D. Wing, V. Giuliano and D. Wing. (1997). Static Investigation of a Fixed-Aperture Nozzle Employing Fluidic Injection for Multiaxis Thrust Vector Control. In *33rd Joint Propulsion Conference and Exhibit*, 3149.

Gu, R. and J. Xu. (2014a). Effects of Cavity on the Performance of Dual Throat Nozzle During the Thrust-Vectoring Starting Transient Process. *Journal of Engineering for Gas Turbines and Power* 136 (1). American Society of Mechanical Engineers. 14502.

Gu, R., J. Xu and S. Guo (2014b). Experimental and Numerical Investigations of a Bypass Dual Throat Nozzle. *Journal of Engineering for Gas Turbines and Power* 136 (8). American Society of Mechanical Engineers Digital Collection.

Gu, R. and J. Xu (2015). Dynamic Experimental Investigations of a Bypass Dual Throat Nozzle. *Journal of Engineering for Gas Turbines and Power* 137 (8). American Society of Mechanical Engineers Digital Collection.

Giuffrida, V., M. Bardi, M. Matrat, A. Robert and G. Pilla (2020). Numerical assessment of ozone addition potential in direct injection compression ignition engines. *International Journal of Engine Research* 1468087420973553.

Hamedi-Estakhrsar, M. H. and H. Mahdavy-Moghaddam (2020a). Experimental Evaluation and Numerical Simulation of Performance of the Bypass Dual Throat Nozzle. *Proceedings of the Institution of Mechanical Engineers, Part G: Journal of Aerospace Engineering*. 0954410020959886.

Hamedi-Estakhrsar, M. H., M. Ferlauto and H. Mahdavy-Moghaddam (2021b). Numerical Study of Secondary Mass Flow Modulation in a Bypass Dual-Throat Nozzle. *Proceedings of the Institution of Mechanical Engineers, Part G: Journal of Aerospace Engineering* 235 (4), 488–500.

Hamedi, H., M. Jahromi, M. Mahmoodi and J. Pirkandi (2015). Effect of Secondary Flow Injection Area on Thrust Vectoring Angle in Double Throat Nozzles. *Modares Mechanical Engineering* 15 (1). 117–125.

Hunter, C. and K. Deere (1999). Computational Investigation of Fluidic Counterflow Thrust Vectoring. In *35th Joint Propulsion Conference and Exhibit*, 2669.

Magnussen, B. F. and B. H. Hjertager (1977). On Mathematical Modeling of Turbulent Combustion with Special Emphasis on Soot Formation and Combustion. In *Symposium (International) on Combustion* 16, 719–729.

Ong, Y. L. F. Salehi, M. Ghiji and V. Garaniya (2021). Numerical study on the effect of injection pressure on high-pressure diesel spray. *Combustion Theory and Modelling* 25, 208–234.

Spalding, D. B. (1971). Mixing and Chemical Reaction in Steady Confined Turbulent Flames. In *Symposium (International) on Combustion* 13, 649–657.

Thillaikumar, T., P. Bhale and M. Kaushik (2020). Experimental Investigations on the Strut Controlled Thrust Vectoring of a Supersonic Nozzle. *Journal of Applied Fluid Mechanics* 13, 1223–1232.

Verma, S., F. Monnier and A. N. Lipatnikov (2021). Validation of leading point concept in RANS simulations of highly turbulent lean syngas-air flames with well-pronounced diffusional-thermal effects. *International Journal of*

Hydrogen Energy 46, 9222–9233.

Waithe, K. and K. Deere (2003). An Experimental and Computational Investigation of Multiple Injection Ports in a Convergent-Divergent Nozzle for Fluidic Thrust Vectoring. In *21st AIAA Applied Aerodynamics Conference*, 3802.

Wang, Y. S., J. L. Xu, S. Huang, Y. C. Lin and J. J. Jiang (2020a). Experimental and Numerical Investigation of an Axisymmetric Divergent Dual Throat Nozzle. *Proceedings of the Institution of Mechanical Engineers, Part G: Journal of Aerospace Engineering* 234 (3), 563–572.

Wang, Y., J. Xu, S. Huang, J. Jiang and R. Pan (2020b). Design and Preliminary Analysis of the Variable Axisymmetric Divergent Bypass Dual Throat Nozzle. *Journal of Fluids Engineering* 142 (6). American Society of Mechanical Engineers Digital Collection.

Wing, D. J. (1994). *Static Investigation of Two Fluidic Thrust-Vectoring Concepts on a Two-Dimensional Convergent-Divergent Nozzle*. Vol. 4574. National Aeronautics and Space Administration, Langley Research Center.

Wing, D. J., and V. J. Giuliano (1997). Fluidic Thrust Vectoring of an Axisymmetric Exhaust Nozzle at Static Conditions. In *ASME Fluids Engineering Division Summer Meeting*, 22–26.

Wu, K. X., T. H. Kim and H. D. Kim (2021). Numerical Study of Fluidic Thrust Vector Control Using Dual Throat Nozzle. *Journal of Applied Fluid Mechanics* 14 (1), 73–87.

Yagle, P. J., D. N. Miller, K. B. Ginn and J. W. Hamstra (2000). Demonstration of Fluidic Throat Skewing for Thrust Vectoring in Structurally Fixed Nozzles. In *Turbo Expo: Power for Land, Sea, and Air*, 78545:V001T01A013. American Society of Mechanical Engineers.